

Chapter 7.

THIN-FILM SILICON SOLAR CELLS

7.1 Introduction

The simplest semiconductor junction that is used in solar cells for separating photo-generated charge carriers is the p - n junction, an interface between the p -type region and n -type region of one semiconductor. Therefore, the basic semiconductor property of a material, the possibility to vary its conductivity by doping, has to be demonstrated first before the material can be considered as a suitable candidate for solar cells. This was the case for amorphous silicon.

The first amorphous silicon layers were reported in 1965 as films of "silicon from silane" deposited in a radio frequency glow discharge¹. Nevertheless, it took more ten years until Spear and LeComber, scientists from Dundee University, demonstrated that amorphous silicon had semiconducting properties by showing that amorphous silicon could be doped n -type and p -type by adding phosphine or diborane to the glow discharge gas mixture, respectively². This was a far-reaching discovery since until that time it had been generally thought that amorphous silicon could not be doped. At that time it was not recognised immediately that hydrogen played an important role in the newly made amorphous silicon doped films. In fact, amorphous silicon suitable for electronic applications, where doping is required, is an alloy of silicon and hydrogen. The electronic-grade amorphous silicon is therefore called **hydrogenated amorphous silicon (a-Si:H)**.

¹ H.F. Sterling and R.C.G. Swann, *Solid-State Electron.* **8** (1965) p. 653-654.

² W. Spear and P. LeComber, *Solid State Comm.* **17** (1975) p. 1193-1196.

The successful doping of amorphous silicon initiated a tremendous interest in this material and the research activities in this field grew explosively all over the world. There were two main reasons for this interest. First, the material had several interesting properties that opened many opportunities for semiconductor device applications. Second, the glow discharge deposition technique enabled the production of *a*-Si:H films over a large area and at a low temperature. At present, this material is for instance used for photoconductive layers in electrophotography, for thin film transistors, and not in the least for solar cells.

Due to a high absorption coefficient of *a*-Si:H in the visible range of the solar spectrum, 1 micrometer (μm) thick *a*-Si:H layer is sufficient to absorb 90% of usable solar light energy. Low processing temperature allows using a wide range of low-cost substrates such as glass sheet, metal or polymer foil. These features has made *a*-Si:H a promising candidate for low-cost **thin-film** solar cells. Low-cost thin-film solar cells are regarded as the second-generation solar cells for terrestrial application.

Since the first *a*-Si:H solar cell made by Carlson and Wronski in 1976, which had an energy conversion efficiency of 2.4%³, the *a*-Si:H solar technology has improved tremendously, leading to present solar cells with initial efficiencies exceeding 15%⁴. Today, amorphous silicon solar cell technology is a matured thin-film solar cell technology that delivered in 2002 *a*-Si:H modules with the total output power of 35.8 MW_p. This represented about 6% of the total PV module production in the world. Recently, experimental modules have been introduced which are based on a combination of *a*-Si:H solar cell and **hydrogenated microcrystalline silicon ($\mu\text{c-Si:H}$)** solar cells. A distinct feature of these solar cells is that all silicon-based layers are deposited in the low-temperature regime ($T < 600^\circ\text{C}$) by plasma assisted chemical vapour deposition techniques. Since in silicon solar cell technology the term “thin-film” usually covers a range of 1 to 100 micrometers thick layers, we refer to the low temperature silicon based solar cells as **thin-film silicon** (TF Si) solar cells.

7.2 Overview of thin-film silicon solar cell technology development

7.2.1 1970-ies

Carlson and Wronski announced the first experimental *a*-Si:H solar cell made at RCA Laboratory in 1976³. This single junction *p-i-n* *a*-Si:H solar cell deposited on a glass substrate coated with transparent conductive oxide (TCO) and aluminium back contact exhibited 2.4% conversion efficiency. In order to increase the output voltage of *a*-Si:H solar cells the concept of a stacked (also called multi-junction) solar cell structure was introduced⁵. A key step to industrial production was the development of a monolithically integrated type of *a*-Si:H solar cell⁶. Using the monolithic series integration of *a*-Si:H solar sub-cells, a desired output

³ D.E. Carlson and C.R. Wronski, *Appl. Phys. Lett.* **28** (1976) p. 671-673.

⁴ J. Yang, A. Banerjee, K. Lord, and S. Guha, *Proceedings of the 2nd World Conference and Exhibition on Photovoltaic Solar Energy Conversion*, Vienna, Austria, July 6 – 10, 1998, p. 387-390.

⁵ Y. Hamakawa, H. Okamoto, Y. Nitta, *Appl. Phys. Lett.* **35**(2) (1979), p. 187-189.

⁶ Y. Kuwano, T. Imai, M. Ohnishi, and S. Nakano, in *Proceedings of the 14th IEEE Photovoltaic Specialist Conference* (1980), p. 1402.

voltage from a single substrate can be easily achieved. In 1980 the integrated type *a*-Si:H solar cells were commercialised by Sanyo and Fuji Electric and applied in consumer electronics, such as calculators and watches.

7.2.2 1980-ies

A large research activity in the field of *a*-Si:H solar cell was devoted to developing and optimising *a*-Si:H based alloys. A *p*-type hydrogenated amorphous silicon carbide (*a*-SiC:H) was implemented as a low-absorbing layer, usually denoted as a window layer⁷, and a hydrogenated amorphous silicon germanium (*a*-SiGe:H) became an attractive low band gap material for stacked solar cells⁸. Surface-textured substrates for optical absorption enhancement were introduced⁹. The laboratory cells reached the initial efficiency in the range of 11 to 12%. Commercial single junction *a*-Si:H modules with efficiencies up to 5% were introduced to the market. The annual production capacity of *a*-Si:H solar cells and modules reached at the end of 1980-ies about 15 MW_p.

7.2.3 1990-ies

The research and manufacturing effort was directed towards achieving 10% stabilized module efficiency and a high throughput process. Several companies optimised and implemented an *a*-SiGe:H alloy in tandem (BP Solar¹⁰, Sanyo¹¹, Fuji Electric¹²) and triple-junction (United Solar¹³) solar cell structures. The annual total production capacity for TF Si single- and multi-junction modules reached around 30 MW_p at the end of the 20th century.

Hydrogenated microcrystalline silicon deposited using the low-temperature PECVD technique emerged in this period as a new candidate for the low band gap material in multi-junction *a*-Si:H based solar cells. The University of Neuchâtel introduced a micromorph tandem solar cell in 1994, which comprised an *a*-Si:H top cell and a μ c-Si:H bottom cell¹⁴. A promising potential of the micromorph cell concept was soon demonstrated by fabricating micromorph tandem and triple solar cells with stabilized efficiencies in the range of 11 to 12%^{15, 16} and Kaneka Corporation started the development of micromorph module production technology¹⁶. The introduction and implementation of μ c-Si:H in TF Si solar cells focused the

⁷ Y. Tawada, H. Okamoto, Y. Hamakawa, *Appl. Phys. Lett.* **39**(3) (1981), p. 237-239.

⁸ G. Nakamura, K. Sato, Y. Yukimoto, K. Shirahata, in *Proceedings of the 3rd E.C. Photovoltaic Solar Energy Conference* (1980), p. 835.

⁹ H.W. Deckman, C.R. Wronski, H. Witzke, and E. Yablonovitch, *Appl. Phys. Lett.* **42**(11) (1983), p. 968.

¹⁰ R.R. Arya and D.E. Carlson, *Progress in Photovoltaics: Research and Applications*, Vol. 10, 2002, p. 69-76.

¹¹ S. Okamoto, A. Terakawa, E. Maruyama, W. Shinohara, M. Tanaka and S. Kiyama, in *Amorphous and Heterogeneous Silicon-Based Films – 2001*, (Mater. Res. Soc. Proc., **664**, San Francisco, CA, 2001), A11.1.

¹² Y. Ichikawa, T. Yoshida, T. Hama, H. Sakai and K. Harashima, *Solar Energy Materials & Solar Cells*, **66** (2001) 107-115.

¹³ S. Guha, J. Yang and A. Banerjee, *Progress in Photovoltaics: Research and Applications*, Vol. 8, 2000, p. 141-150.

¹⁴ J. Meier, S. Dubail, R. Flückiger, D. Fischer, H. Keppner, A. Shah, in *Proceedings of the 1st World Conference on Photovoltaic Energy Conversion* (1994), p.409-412.

¹⁵ J. Meier, S. Dubail, J. Cuperus, U. Kroll, R. Platz, P. Torres, J.A. Anna Selvan, P. Pernet, N. Beck, N. Pellaton Vaucher, Ch. Hof, D. Fischer, H. Keppner, A. Shah, *J. Non-Cryst. Solids* **227-230** (1998) 1250-1256.

¹⁶ K. Yamamoto, M. Yoshimi, Y. Tawada, Y. Okamoto, A. Nakajima, *J. Non-Cryst. Solids* **266-269** (2000) 1082-1087.

attention upon the increase of the deposition rate. Several new deposition methods¹⁷ have been investigated for fabrication of solar cells at high deposition rates (0.5 to 1.0 nm/s), such as very high frequency and microwave PECVD, hot wire CVD, and expanding thermal plasma CVD.

7.3 Hydrogenated amorphous silicon

In order to understand design and operation of an *a*-Si:H solar cell, which is different from a crystalline silicon (c-Si) cell, the material properties of *a*-Si:H are summarised and compared to the single crystal silicon.

7.3.1 Atomic structure

Figure 7.1 illustrates the difference in the atomic structure between single crystal silicon and *a*-Si:H. Figure 7.1a shows the structure of single crystal silicon schematically. Each Si atom is covalently bonded to four neighbouring Si atoms. All bonds have the same length and the angles between the bonds are equal. The number of bonds that an atom has with its immediate neighbours in the atomic structure is called the **coordination number** or **coordination**. Thus, in single crystal silicon, the coordination number for all Si atoms is four; we can also say that Si atoms are fourfold coordinated. A **unit cell** can be defined, from which the crystal lattice can be reproduced by duplicating the unit cell and stacking the duplicates next to each other. Such a regular atomic arrangement is described as a structure with **long range order**. A diamond lattice unit cell represents the real lattice structure of single crystal silicon.

Figure 7.1b illustrates that *a*-Si:H does not exhibit the structural order over a long-range as is the case for single crystal silicon. Nevertheless, there is a similarity in atomic configuration on a local atomic scale, where most Si atoms have covalent bonds with four neighbours. The *a*-Si:H has the same **short-range order** as the single crystal silicon but it lacks the long range order. The small deviations in bonding angles and bonding lengths between the neighbouring atoms in *a*-Si:H lead to a complete loss of the locally ordered structure on a scale exceeding a few atomic distances. The resulting atomic structure of *a*-Si:H is called the **continuous random network**. Due to the short-range order in the continuous random network of *a*-Si:H, the common semiconductor concept of the energy states bands, represented by the conduction and valence bands, can still be used.

The larger deviations in bonding angles and bonding lengths between the neighbouring atoms in *a*-Si:H result in the so-called **weak** or **strained bonds**. The energy of the weak bonds is higher than the energy of optimal silicon covalent bonds in ideal single crystal silicon. Therefore, the weak bonds can easily break and form **defects** in the atomic network. We note that in the continuous random network, the definition of a defect is modified with respect to the crystal structure. In a crystal any atom that is out of place in a lattice forms a defect. In the continuous random network an atom cannot be out of place. Because the only specific structural feature of an atom in the continuous random network

¹⁷ R.E.I. Schropp and M. Zeman, *Amorphous and Microcrystalline Solar Cells: Modeling, Materials, and Device Technology*, Kluwer Academic Publishers, 1998.

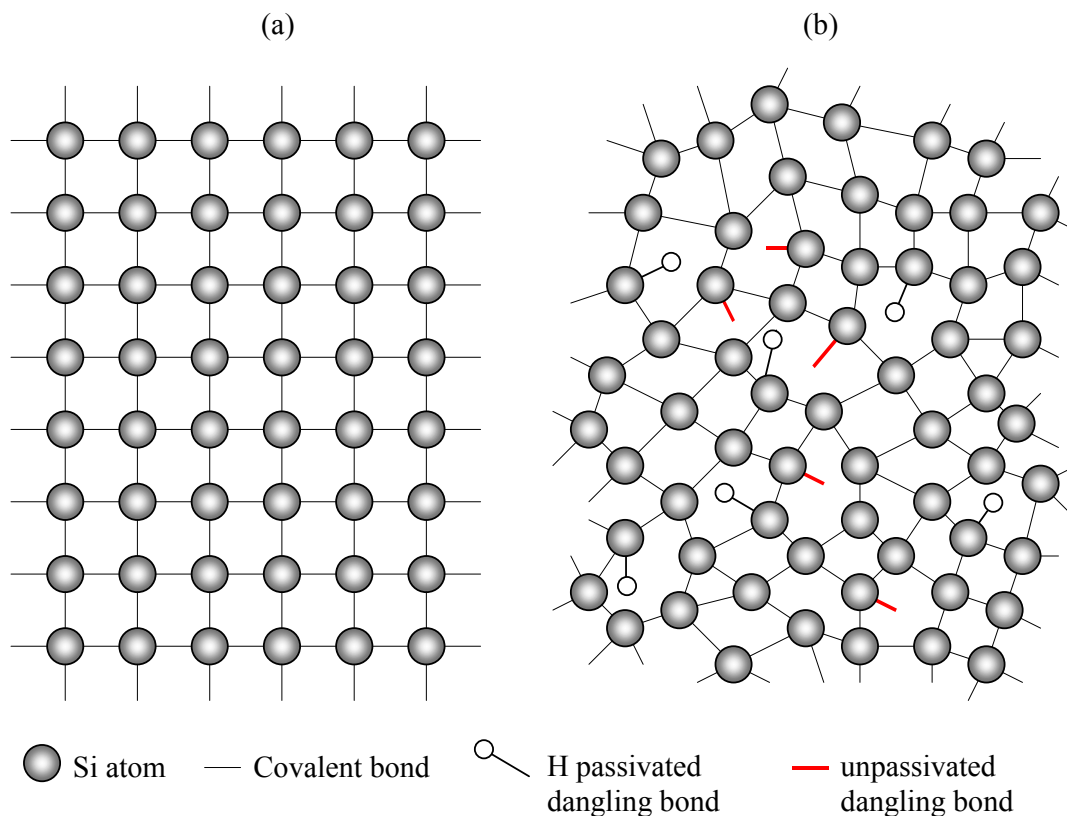


Figure 7.1. Schematic representation of the atomic structure of (a) single crystal silicon (b) hydrogenated amorphous silicon.

is the coordination to its neighbours, a defect in *a*-Si:H is the **coordination defect**. This happens when an atom has too many or too few bonds. In *a*-Si:H the defects are mainly represented by Si atoms that are covalently bonded to only three Si atoms (**threefold coordinated**) and have one unpaired electron, a so-called **dangling bond**. Since this configuration is the dominant defect in *a*-Si:H, the defects in *a*-Si:H are often related to the dangling bonds.

When amorphous silicon is deposited in such a way that hydrogen can be incorporated in the network (as in the case of glow discharge deposition from silane), then the hydrogen atoms bond with most of the dangling bonds. We say that the dangling bonds are **passivated** by hydrogen. Hydrogen passivation reduces the dangling bond density from about 10^{21} cm^{-3} in pure *a*-Si (amorphous silicon that contains no hydrogen) to 10^{15} - 10^{16} cm^{-3} in *a*-Si:H, i.e. less than one dangling bond per million Si atoms. In Fig. 1b some of the defects with unpassivated dangling bonds and with hydrogen passivated dangling bonds are depicted. Device quality *a*-Si:H contains from 1 to 10 atomic percent of hydrogen. In summary, the short range order in *a*-Si:H network and the hydrogen passivation of the dangling bonds are responsible for semiconductor properties of amorphous silicon.

7.3.2 Density of energy states

The difference in the atomic structure between single crystal silicon and *a*-Si:H leads to the different distributions of density of allowed energy states as schematically illustrated in Figure 7.2. The periodic atomic structure of single crystal silicon results in the ranges of allowed energy states for electrons that are called **energy bands** and the excluded energy ranges, **forbidden gaps** or **band gaps**. Figure 2a shows schematically the distribution of density of states for single crystal silicon, in which the valence band and the conduction band are separated by a well-defined band gap, E_g . At room temperature single crystal silicon has a band gap of 1.12 eV. In case of an ideal crystal, there are no allowed energy states in the band gap.

As Figure 7.2b demonstrates, in case of *a*-Si:H, there is a continuous distribution of density of states and no well defined band gap exists between the valence band and the conduction band. Due to the long range order disorder in the atomic structure of *a*-Si:H the energy states of the valence band and the conduction bands spread into the band gap and form regions that are called **band tail** states. The band tail states represent the energy states of electrons that form the strained bonds in the *a*-Si:H network. The width of the band tails is a measure for the amount of disorder in *a*-Si:H material. More disorder in *a*-Si:H means that the band tails are broader. In addition, the dangling bonds introduce allowed energy states that are located in the central region between the valence band and conduction band states.

The electron and hole wavefunctions that extend over the whole structure are characteristic for energy states, in which the charge carriers can be considered as free carriers. These states are non-localised and are called **extended states**. The wavefunctions of the tail and defect states are localized within the structure and therefore these states are called **localised states**. Consequently, mobility that characterises transport of carriers through the

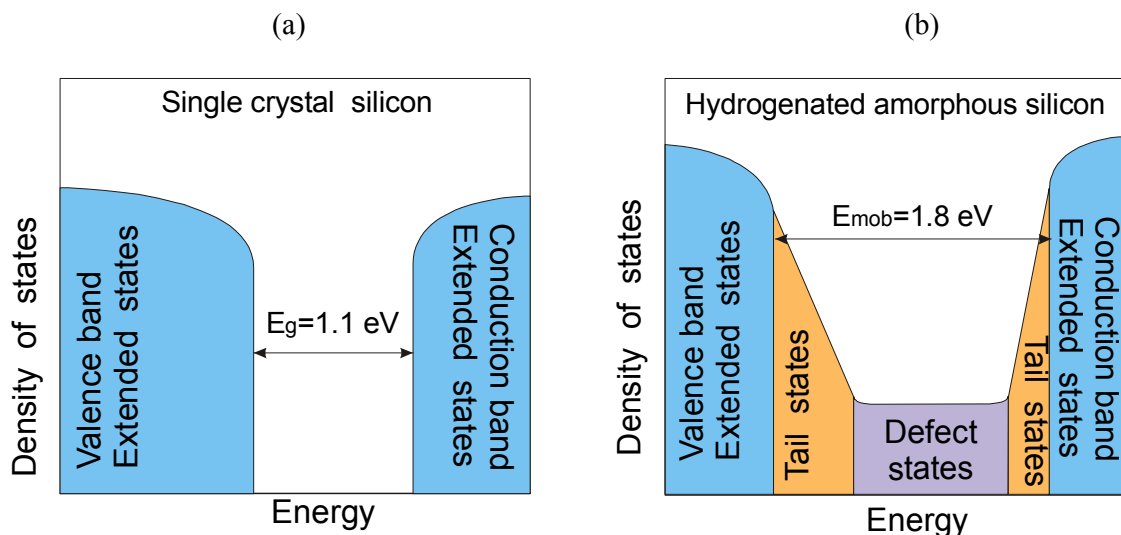


Figure 7.2. The schematic representation of the distribution of density of allowed energy states for electrons for (a) single crystal silicon (b) *a*-Si:H.

localised states is strongly reduced. This feature of a sharp drop of mobility of carriers in the localised states in *a*-Si:H is used to define its band gap. This band gap is denoted by the term **mobility gap**, E_{mob} , because the presence of a considerable density of states in this gap conflicts the classical concept of the band gap. The energy levels that separate the extended states from the localised states in *a*-Si:H are called the valence band and the conduction band mobility edges. The mobility gap of *a*-Si:H is larger than the band gap of single crystal silicon and has a typical value of 1.8 eV. The localised tail and dangling bond states have a large effect on the electronic properties of *a*-Si:H. The tail states act as trapping centres and build up a space charge in a device, the dangling bond states act as very effective recombination centres and affect in particular the lifetime of the charge carries.

7.3.3 Optical properties

The optical properties of *a*-Si:H are usually characterised by its **absorption coefficient** and a value of the **optical band gap**. Figure 7.3a shows the absorption coefficient of *a*-Si:H that is fabricated at Delft University of Technology as a function of photon energy. The absorption coefficient of c-Si is shown for reference. This figure demonstrates that *a*-Si:H absorbs almost 100 times more than c-Si in the visible part of the solar spectrum. The higher absorption is due to the disorder in the atomic structure of *a*-Si:H that behaves like a direct gap semiconductor. This means that 1 μm thick *a*-Si:H layer is sufficient to absorb 90% of usable solar light energy. In practice the thickness of *a*-Si:H solar cells is less than 0.5 μm that is about 100 times less than the thickness of a typical single crystal silicon cell. This results in important savings in both material and energy in fabrication of *a*-Si:H solar cells.

Another advantage of *a*-Si:H is that the optical absorption can be slightly changed by varying its hydrogen content, and it can be greatly changed by **alloying** with carbon or germanium. The absorption coefficient of hydrogenated amorphous silicon carbide (*a*-SiC:H) and hydrogenated amorphous silicon germanium (*a*-SiGe:H) that are fabricated at Delft University of Technology are also shown in Figure 7.3a. This feature of easy alloying of *a*-Si:H allows to design solar cell structures in which *a*-Si:H based materials with different absorption properties can be used as active layers.

From the absorption coefficient of *a*-Si:H based materials, the so called optical band gap is determined. The optical band gap is a useful material parameter that allows comparison of *a*-Si:H based materials regarding their light absorption properties. In general, a material with higher optical band gap absorbs less. The optical band gap, E_{opt} , is determined by extrapolating a linear part of the following function $[\alpha(E) \times n(E) \times E]^{1/(1+p+q)}$ vs the photon energy E to $\alpha(E) = 0$, for $\alpha \geq 10^3 \text{ cm}^{-1}$:

$$(\alpha(E) \times n(E) \times E)^{1/(1+p+q)} = B(E - E_{opt}) \quad (7.1)$$

where $\alpha(E)$ is the absorption coefficient, $n(E)$ is the refractive index, p and q are constants that describe the shape of the density of extended states distribution for the conduction band and valence band, respectively, and B is a prefactor. When the density of states distribution near the band edges has a square-root energy dependence ($p=q=1/2$), as is commonly the case in crystalline semiconductors, Eq. 1 describes the so-called Tauc plot and the corresponding

(a)

(b)

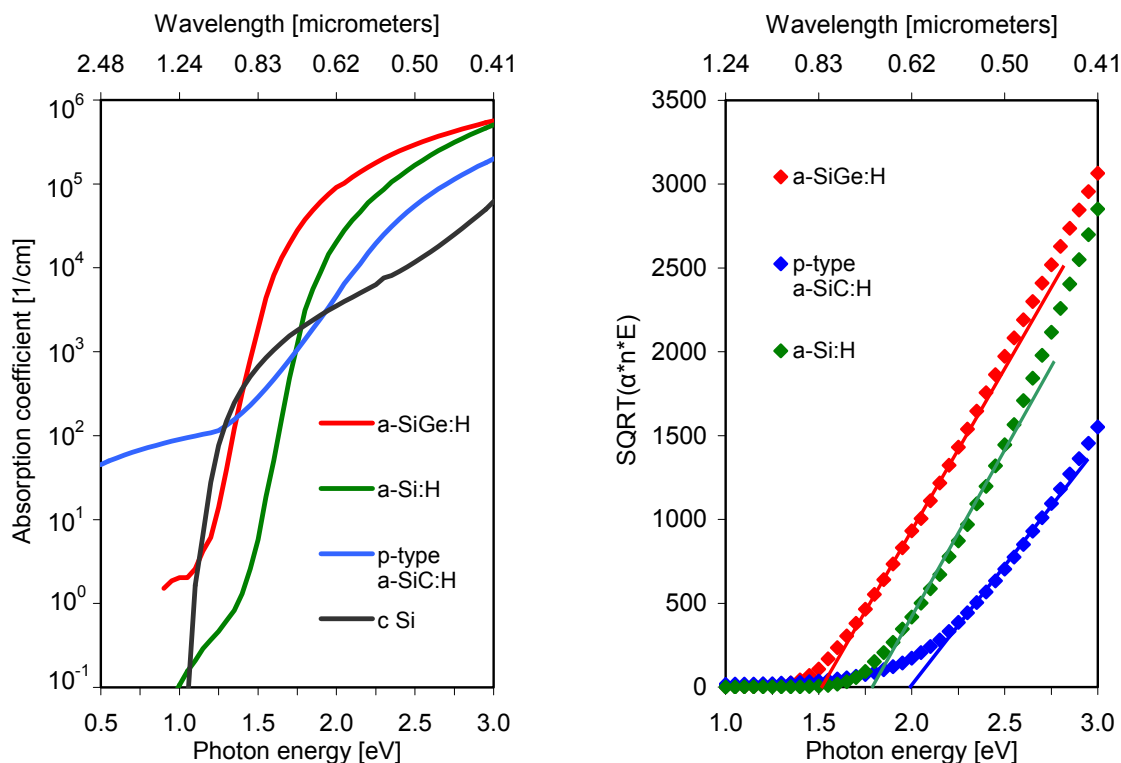


Figure 7.3. (a) Absorption coefficient as function of photon energy for *a*-Si:H, *p*-type *a*-SiC:H and *a*-SiGe:H fabricated at Delft University of Technology. The absorption coefficient of *c*-Si is shown for reference. (b) Tauc plot with linear extrapolation to determine the Tauc optical band gap for *a*-Si:H, *p*-type *a*-SiC:H and *a*-SiGe:H.

optical band gap is called the **Tauc optical gap**. When the distribution near the band edges is assumed to be linear ($p=q=1$) E_{opt} is called the **cubic optical gap**. The Tauc gap of device quality intrinsic *a*-Si:H is in the range of 1.70 to 1.80 eV, the cubic gap of the same material is usually 0.1 to 0.2 eV smaller than the Tauc gap. The Tauc plot with linear extrapolation to determine the Tauc optical gap for *a*-Si:H ($E_{opt}=1.77$ eV), *p*-type *a*-SiC:H ($E_{opt}=1.95$ eV), and *a*-SiGe:H ($E_{opt}=1.52$ eV) is shown in Figure 7.3b.

7.3.4 Electrical properties

The electrical properties of *a*-Si:H are usually characterised in terms of dark conductivity and photoconductivity. The measurement of these two properties is a standard approach to obtain information about the quality of *a*-Si:H material for application in solar cells. Also it gives information about the mobility-lifetime product and the influence of impurities in *a*-Si:H. The mobilities of the charge carriers in the extended states of *a*-Si:H are about two orders of magnitude lower than in single crystal silicon. Typically, the electron mobility is $10 \text{ cm}^2/\text{Vs}$, and the hole mobility is $1 \text{ cm}^2/\text{Vs}$ in intrinsic *a*-Si:H. The low values

of electron and hole mobilities and the high mobility gap of a -Si:H result in a low dark conductivity, which in device quality intrinsic a -Si:H is less than $1 \times 10^{-10} \Omega^{-1} \text{ cm}^{-1}$. This material is further characterised by an excellent photoconductivity that is higher than $1 \times 10^{-5} \Omega^{-1} \text{ cm}^{-1}$, when measured using the AM1.5 light spectrum and the incident power of 100 mW/cm^2 .

7.3.5 Doping of a -Si:H

The purpose of doping is to manipulate the type of electrical conductivity and its magnitude by adding a controlled amount of special impurity atoms. The principal doping elements used in a -Si:H are the same as in crystalline silicon: boron for p -type and phosphorus for n -type material. The doped layers have two functions in an a -Si:H solar cell. First, they set up an internal electric field across the active intrinsic a -Si:H layer. The electric field should be high enough to ensure that the photo-generated carriers in intrinsic a -Si:H layer are collected. The strength of the electric field depends on the level of doping in the doped layers and the thickness of the intrinsic layer. Second, they establish low-loss ohmic electrical contacts between the a -Si:H part of solar cell and the external electrodes.

Spear and LeComber from Dundee University reported in 1975 that amorphous silicon could be doped by addition of boron and phosphorus. They achieved the change in conductivity of a -Si:H by mixing the silicon source gas, silane (SiH_4), with phosphine (PH_3) or diborane (B_2H_6) during the deposition using the glow discharge method. Figure 7.4 shows the room temperature conductivity, σ_{RT} , of their a -Si:H as a function of fraction of doping gases in a mixture with silane². The conductivity of a -Si:H could be varied by more than a factor 10^8 . The activation energy decreases from 0.7 - 0.8 eV in intrinsic material to about 0.15 eV in phosphorus doped material and 0.3 eV in boron doped material.

The demonstration of effective doping of a -Si:H was an important breakthrough, because the researchers believed for a long time that the effective doping of amorphous silicon could not be achieved. They assumed that the continuous random network could easily incorporate impurity atoms, such as phosphorus and boron, with coordination that corresponded to the bonding configuration with the lowest energy. This property of the continuous random network is in contrast to the crystalline structure, in which, due to the long range order, the impurity atoms are forced to adopt the coordination of the host atoms. In the continuous random network the optimum number of covalent bonds (coordination), Z , for an atom with N valence electrons is,

$$\begin{aligned} Z &= 8 - N && \text{for } N \geq 4 \\ Z &= N && \text{for } N < 4. \end{aligned}$$

This prediction of the atom coordination in the continuous random network is known as the **8-N rule** and was introduced by Mott in 1969¹⁸.

¹⁸ N.F. Mott, *Philos. Mag.* **19** 835 (1969).

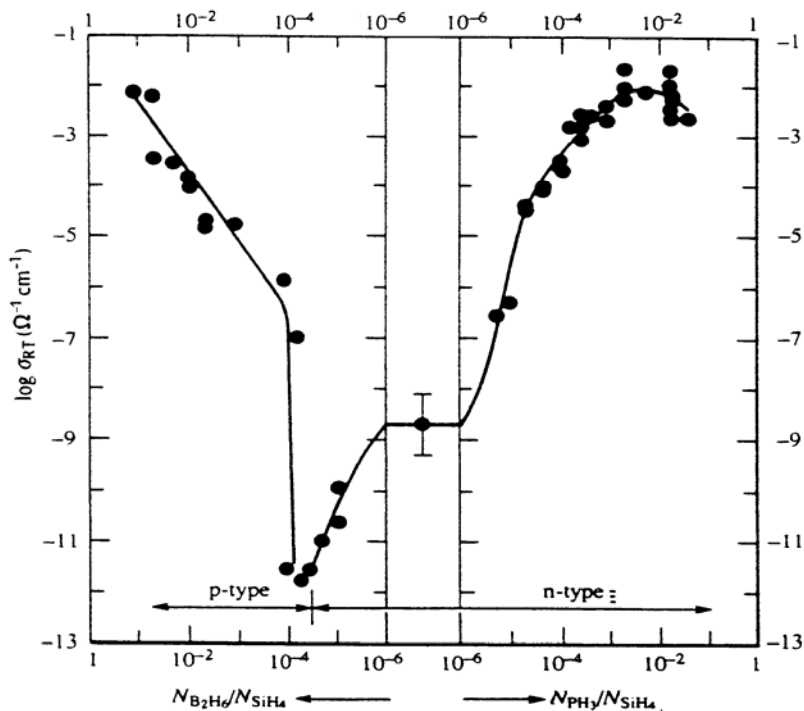


Figure 7.4. Room-temperature conductivity σ_{RT} of n - and p -type amorphous silicon, plotted as a function of the ratio between the numbers of doping gases molecules and silane molecules in the gas mixture².

For example, following the $8-N$ rule a phosphorus atom with five valence electrons would incorporate itself in the continuous random network by forming three covalent bonds with neighbouring atoms. This situation is illustrated in Figure 7.5a. In order to describe the configuration of the atoms in the structural network notation T_z^q is used. T is the atom, z is the coordination number, and q is the charge state of the atom. P_3^0 denotes a phosphorus atom that is covalently bonded to three neighbouring atoms and is neutral. In a -Si:H most of the phosphorus atoms are incorporated according to the $8-N$ rule. They adopt the optimal threefold coordination that represents the **non-doping state** and thus is electrically inactive. The doping efficiency in a -Si:H, which is defined as the fraction of dopant atoms with fourfold coordination, is rather low. In comparison to single crystal silicon, where the doping efficiency at room temperature is almost unity, it is in the range of 10^{-2} - 10^{-3} in a -Si:H. This means that relatively high concentrations of phosphorous atoms must be introduced in order to obtain material with high conductivity. A phosphorous atom can also be incorporated as the neutral donor P_4^0 in the network as it is the case in single crystal silicon (see Figure 7.5c), but this configuration is characterised by much higher energy than the optimal P_3^0 configuration and therefore is unstable in the continuous random network. Most of the phosphorous atoms, which contribute to doping, are not P_4^0 neutral donors, but charged phosphorus atoms P_4^+ . The formation of the P_4^+ charged state is accompanied by formation of negatively charged dangling bond Si_3^- as it is illustrated in Fig. 5b. The P_4^+ and Si_3^- configuration is energetically more favourable than P_4^0 donor and is called the **defect-compensated donor**.

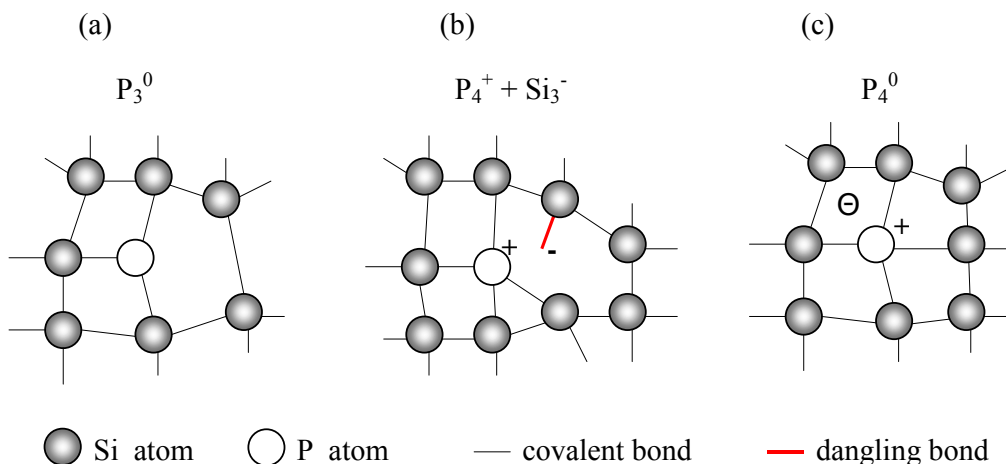


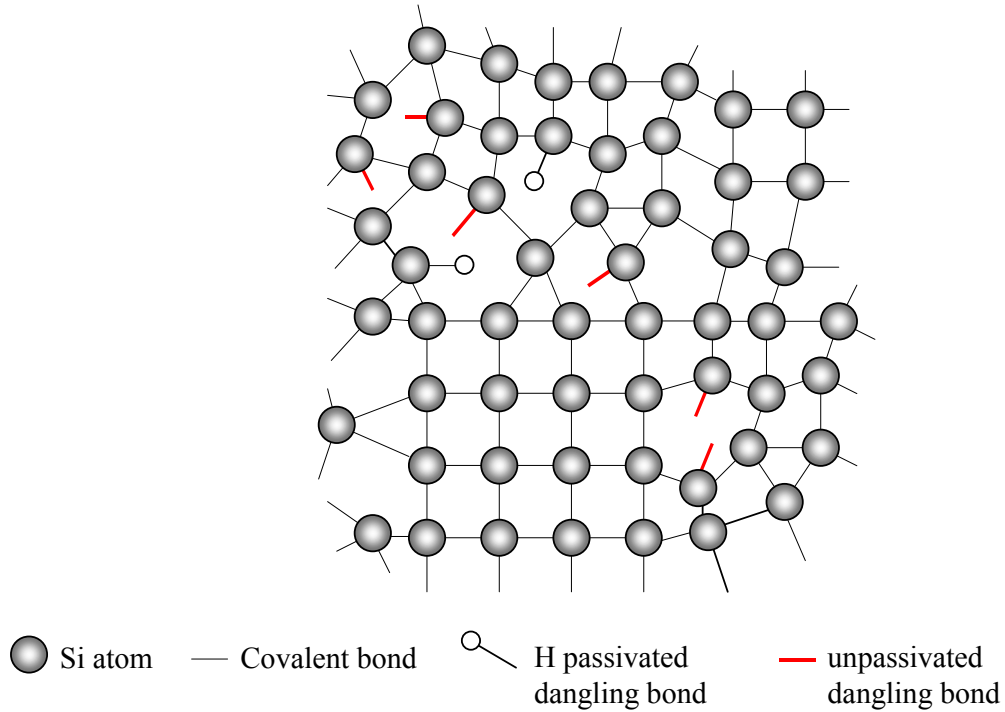
Figure 7.5. Possible configurations of a phosphorous atom in a -Si:H network. (a) the non-doping state P_3^0 , (b) the defect-compensated donor state $P_4^+ + Si_3^-$, (c) the neutral donor P_4^0 .

The formation of the defect-compensated donors in the case of phosphorus atoms and defect compensated acceptors in the case of boron atoms is the major doping mechanism in a -Si:H. This mechanism was explained by Street and it is known as the **autocompensation model**¹⁹. The most important result of this model is that doping of a -Si:H inevitably leads to creation of dangling bonds. Doped a -Si:H has two or three orders of magnitude larger defect density in comparison to intrinsic a -Si:H. The diffusion length of charge carriers in doped a -Si:H is very small compared to single crystal silicon. For this reason a -Si:H solar cells cannot function successfully as a p - n junction but a relatively defect free intrinsic layer has to be inserted between the p -type and n -type layers. Because the underlying processes of the photovoltaic effect such as absorption of light and separation of photo-generated carriers take place in the intrinsic layer, this layer is called an active layer in a -Si:H solar cell.

An additional important difference between a -Si:H and single crystal silicon is that when increasing the concentration of boron and phosphorous doping atoms in a -Si:H, the Fermi level does not move closer to the valence band mobility edge than 0.30 eV and 0.15 eV to the conduction band mobility edge, respectively. The reason for this is that the shift of the Fermi level towards the band edges decreases the probability of forming the doping state configurations and favours the non-doping configurations. Further, when the Fermi level is shifted towards the band edges it is located in the band tail states, which density increases exponentially towards the mobility band edges. Therefore any further shift towards the band edges is accompanied by building up of a large space charge in the tail states that compensates the charge created by ionised doping atoms.

¹⁹ R.A. Street, *Phys. Rev. Lett.* **49** 1187 (1982).

7.4 Hydrogenated microcrystalline silicon



This figure shows a schematic structural representation of hydrogenated microcrystalline silicon ($\mu\text{c-Si:H}$). Small crystals of highly ordered material in the range of tenths of nanometres are imbedded in the amorphous structure.

7.5 Deposition of thin-film silicon

The methods that are used for depositing thin films of a -Si:H and μc -Si:H can be divided in two groups. The first group includes methods that form a -Si:H and μc -Si:H from a gas phase by decomposition of silicon-bearing gas, usually SiH_4 . These methods are known as **chemical vapour deposition** (CVD) methods. The second group represents the physical deposition methods in which silicon atoms for a -Si:H growth are obtained by sputtering a silicon target.

7.5.1 Plasma Enhanced Chemical Vapour Deposition

The most commonly used deposition method to produce "device quality" a -Si:H, both on the laboratory and industrial scale, is the radio frequency (13.56 MHz) plasma decomposition of SiH_4 , known as the Plasma Enhanced CVD (rf PECVD) method or the glow discharge (GD) deposition. The PECVD deposition system is schematically shown in Figure 7.6. The role of the plasma is to provide a source of energy to dissociate the SiH_4 molecules. This is done by collisions with electrons, which originate as secondary electrons in the plasma and build up their energy by acceleration in an electric field. The growth of an a -Si:H film is accomplished by attachment of reactive particles of dissociated SiH_4 molecules, called radicals, to the surface of the growing film. As the thickness of the a -Si:H film for device applications is around half a micrometer, a -Si:H must be deposited on an appropriate substrate carrier. Some of the energy transferred to the SiH_4 molecules in the collisions with electrons is radiated as visible light, hence the deposition method is also called the glow discharge.

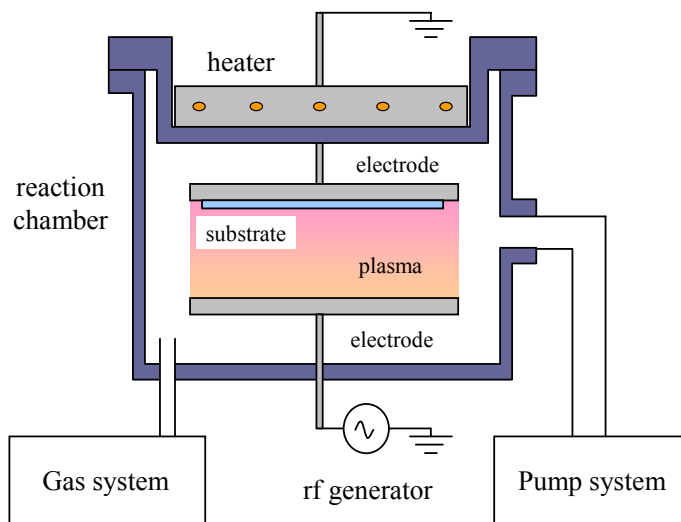


Figure 7.6. The schematic representation of a rf PECVD deposition system.

The PECVD deposition system is relatively simple and consists of five main parts (see Figure 7.6):

- reaction chamber with the capacitatively coupled parallel electrodes
- vacuum pump system
- gas handling system
- dc or rf power source
- substrate heating assembly

The deposition temperature of device quality *a*-Si:H is usually between 200°C and 250°C. This temperature range allows using a wide range of low cost substrates (glass, stainless steel, flexible plastic foils, or ceramic). The deposition process can be scaled up to large area substrates (more than 1 m²). However, scaling requires a careful design of reactor geometry in order to produce uniform and homogeneous films. Doping and alloying of *a*-Si:H is simply accomplished by adding appropriate gases to the source gas mixture. For instance, in order to make *p*-type material B₂H₆ is added to the gas mixture and boron is incorporated in the material, for *n*-type material PH₃ is used in the gas mixture. Adding germane (GeH₄) or methane (CH₄) to the gas mixture results in *a*-SiGe:H material with a lower optical band gap or *a*-SiC:H material with higher optical band gap, respectively.

The advantages of rf PECVD deposition technology are briefly summarised:

- large area deposition (more than 1 m²)
- low deposition temperature (100°C < T_s < 400°C)
- use of any cheap and arbitrarily shaped substrates
- effective *p*- and *n*-type doping and alloying
- deposition of composition-graded layers
- deposition of multi-layer structures by control of gas mixtures in a continuous process
- easy patterning and integration technology
- low cost
- good mass-productibility

7.5.2 High deposition rate techniques

At present *a*-Si:H solar cells are mainly produced by the rf PECVD process. This process has also been successfully applied for the mass production of large area solar cells. A drawback of the rf PECVD technique is a relatively low deposition rate. The device quality material that is required for high-efficiency solar cells is obtained at a typical deposition rate of 2-5 Å/s. However, for high volume production it is somewhat low and therefore considerable research effort is devoted to high-rate deposition methods of *a*-Si:H layers. Several novel deposition methods are investigated, e.g., hot filament assisted CVD, known also as hot wire CVD (HW-CVD) technique at Utrecht University and the expanding thermal plasma CVD (ETP-CVD) technique developed at Eindhoven University of Technology.

HW CVD is based on the dissociation of a gas by catalytic action of a hot filament. Similar deposition systems can be used as in case of rf PECVD in Fig. 7.6; only the reaction chamber is modified. Instead of two parallel electrodes, filaments are introduced into the chamber and placed in the vicinity of the substrate holder. The filaments are made of tungsten or tantalum. The decomposition of SiH₄ into single silicon and hydrogen radicals is efficient

for filament temperatures above 1600°C. The a-Si:H layers are typically deposited at 250°C to 350°C with a deposition rate of 10 Å/s.

The ETP deposition set-up is shown in Figure 7.7a. The set-up consists of a dc thermal-arc plasma source and a low-pressure deposition chamber. The plasma generation and film deposition are separated and this system is therefore regarded as a remote-plasma system. The plasma is generated in a gas mixture of argon and hydrogen by a dc discharge (typically 50 A, 100 V). The pressure in the plasma source is ~200 mbar, from which the plasma expands supersonically into the deposition chamber, where the pressure is typically 0.2 mbar. Pure SiH₄ is injected into the plasma jet just behind the expansion nozzle. The deposition rate is dependent on a number of factors, such as the pressure in the deposition chamber and SiH₄ flow, and can reach 1000 Å/s. In order to employ the ETP deposition method for a-Si:H solar cells, at Delft University of Technology a system has been built, called CASCADE, in which a complete solar cell can be fabricated. The system consists of three chambers: an rf PECVD chamber for the deposition of the doped layers, an ETP chamber for the high-rate deposition of the intrinsic layer, and a load-lock. The ETP deposition chamber is shown in Figure 7.7b. The doped layers are produced using PECVD, because an accurate control of the thickness of these layers is essential and thus a fairly low deposition rate is desired.

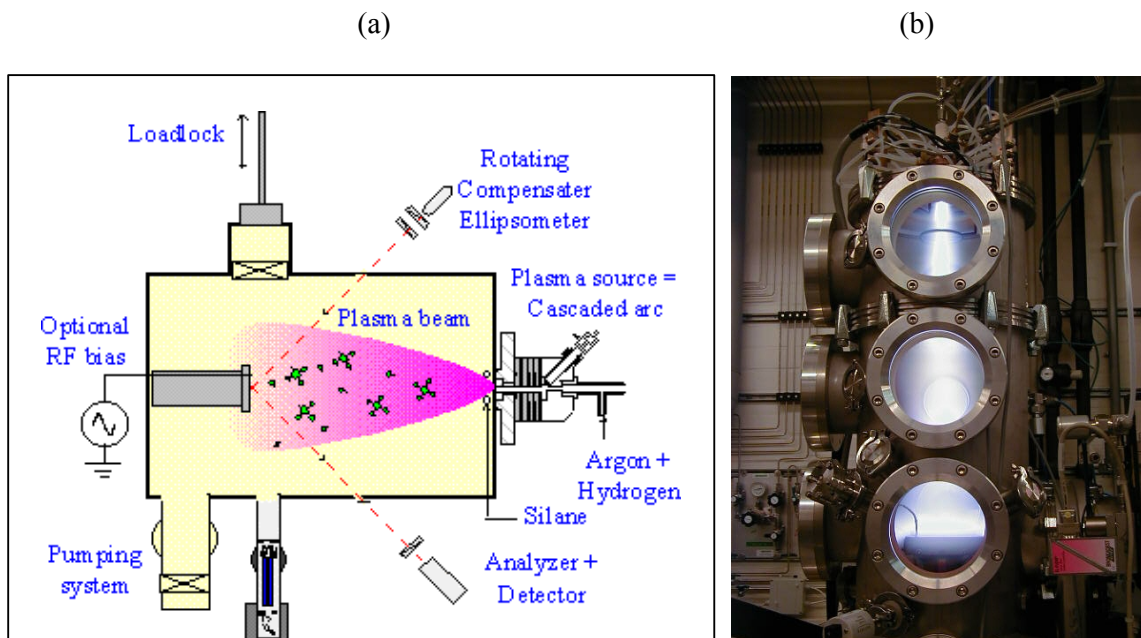


Figure 7.7. (a) A schematic representation of the ETP deposition system. (b) A photograph of the ETP chamber of the CASCADE deposition system at Delft University of Technology during operation.

7.6 Thin-film silicon solar cells

7.6.1 Comparison of c-Si and *a*-Si:H solar cells

There is a fundamental difference between c-Si and *a*-Si:H solar cells. A typical c-Si solar cell, shown in Figure 7.8a, consists of a *p*-type wafer, which is 300 to 500 μm thick, with a thin *n*-type layer on the top of the wafer, which forms a *p-n* junction. The width of the depletion region of the *p-n* junction is less than 0.5 μm . The depletion region, where an internal electric field is created, represents only a tiny part of the wafer. Most electron-hole pairs are generated in the bulk of the electrically neutral *p*-type region. Electrons, which are the minority carriers in the *p*-type region, diffuse towards the *p-n* junction and in the depletion region of the junction the electrons drift to the *n*-type layer under the influence of the internal electric field. This solar cell is called a *diffusion device* because the dominant transport mechanism of the photo-generated carriers is diffusion. Therefore, the diffusion length of minority carriers (i.e. electrons in *p*-type material) is an important material parameter that determines design and performance of c-Si solar cells. Typical values of the diffusion length of electrons in the *p*-type float zone single crystal silicon wafers are in the range of 250 μm to 700 μm . These values correspond to wafers with a resistivity in the range of 0.25 to 1.0 $\Omega\text{ cm}$, respectively.

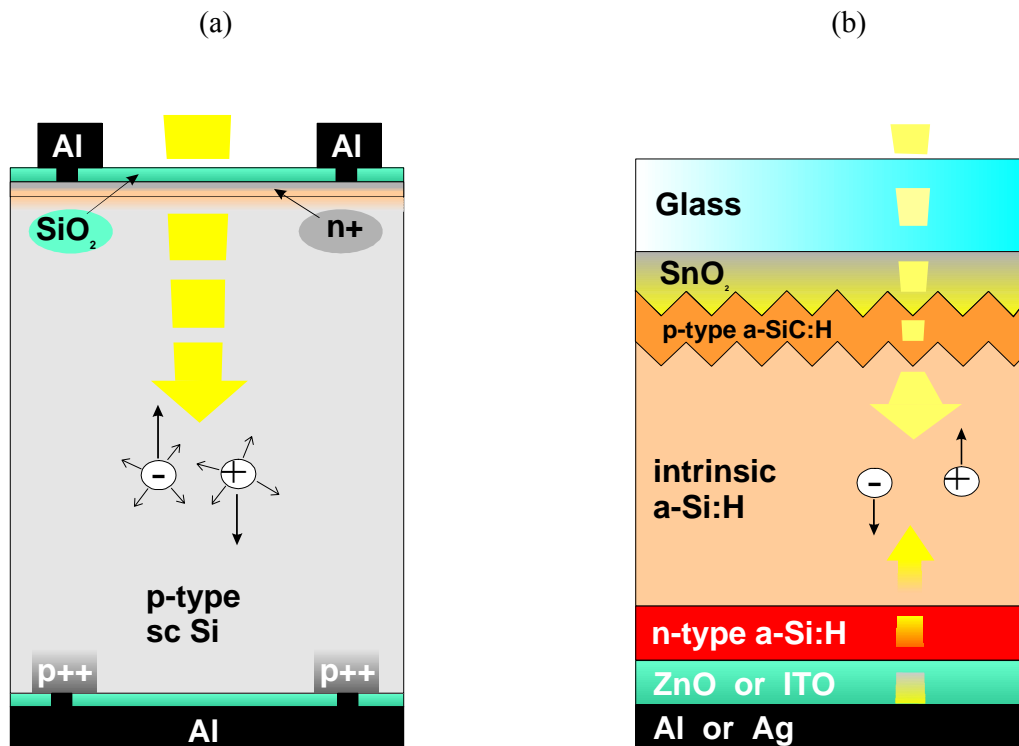


Figure 7.8. A typical structure of (a) c-Si solar cell and (b) *a*-Si:H solar cell.

In a -Si:H the diffusion length of the charge carriers is much shorter than in single crystal silicon. In device quality intrinsic a -Si:H the ambipolar diffusion length ranges from 0.1 to 0.3 μm . In doped a -Si:H layers, in which the defect density due to the doping is two or three orders of magnitude higher than in the intrinsic a -Si:H, the diffusion length of the minority carriers is much lower. A solar cell structure based on the diffusion of the minority carriers in the electrically neutral regions of the doped layers as in the case of c-Si does not work in the case of a -Si:H. The photo-generated carriers would all recombine in the doped layers before reaching the depletion region of the p - n junction due to the very short diffusion length. Therefore, an a -Si:H solar cell is designed differently. A schematic lay-out of an a -Si:H solar cell is shown in Figure 7.8b. The active device consists of three layers: a p -type a -SiC:H layer, an intrinsic a -Si:H layer, and an n -type a -Si:H layer. The doped layers are usually very thin, a p -type a -SiC:H layer is ~ 10 nm thick and an n -type a -Si:H is ~ 20 nm thick. The active layer in the a -Si:H solar cell is the intrinsic layer which is typically 300 to 500 nm thick. This intrinsic layer is sandwiched in between the doped layers so that an internal electric field is present across the intrinsic layer. The electron-hole pairs that are generated in the intrinsic a -Si:H layer immediately experience the internal electric field that separates electrons and holes from each other. The separated carriers drift under the influence of the internal electric field towards the doped layers (electrons towards the n -type layer and holes towards the p -type layer) and are collected by the electrodes. The dominant transport mechanism of the photo-generated carriers is drift in the internal electric field and therefore an a -Si:H solar cell is called a *drift device*. A stack, which consists of p -type a -SiC:H, intrinsic a -Si:H and n -type a -Si:H layers, forms the p - i - n junction. This structure of a -Si:H solar cell is presented in Figure 7.8b and it is generally called a *single junction* a -Si:H solar cell. The band diagrams of c-Si and single junction a -Si:H solar cells are presented in Figure 7.9a and 7.9b, respectively, which also demonstrate the difference between the diffusion type and the drift type solar cell.

The thickness of the a -Si:H solar cell is comparable to the thickness of the depletion region in the crystalline silicon solar cell, i.e. about 0.5 μm . As mentioned earlier, this small thickness is sufficient for absorption of the visible part of solar radiation. The small thickness implies a large reduction in material and energy consumption during production when compared to crystalline silicon solar cells. Furthermore, when deposited on a light substrate such as a flexible foil the weight of a -Si:H solar modules is strongly decreased. This is desired specifically in space applications. The thicknesses of individual layers in c-Si and a -Si:H solar cells are compared in Table 7.1.

Table 7.1. Comparison of the thicknesses of individual layers in c-Si and a -Si:H solar cells.

Crystalline silicon solar cell		a -Si:H solar cell	
Al contact	0.5 to 1.0 μm	top glass	2 to 4 mm
SiO ₂ or Si ₃ N ₄ layer	~ 0.1 μm	transparent electrode	0.5 to 0.9 μm
n^+ -type emitter	0.3 to 0.5 μm	p -type a -SiC:H	0.01 μm
p-type base	300 to 500 μm	intrinsic a-Si:H	0.3 to 0.5 μm
p^+ -type region	1.0 μm	n -type a -Si:H	0.02 μm
SiO ₂ layer	0.05 to 0.1 μm	ZnO or ITO layer	~ 0.1 μm
Al contact	0.5 to 1.0 μm	Al or Ag contact	0.5 to 1.0 μm

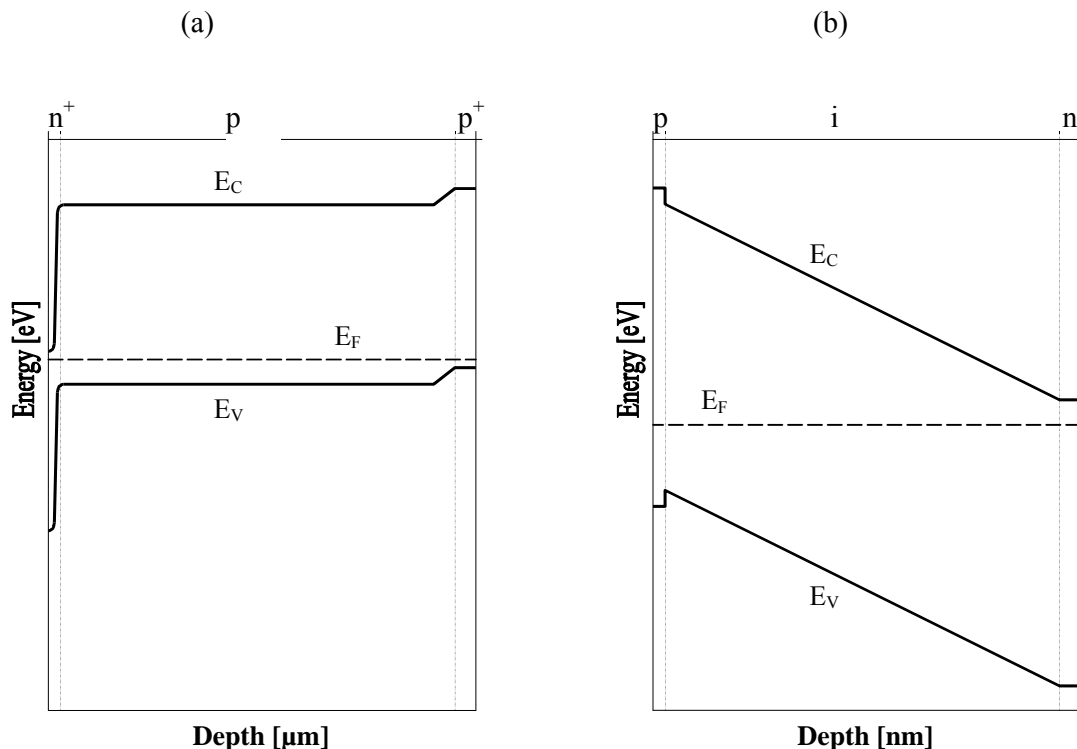


Figure 7.9. Band diagram of (a) c-Si solar cell and (b) single junction *a*-Si:H solar cell.

Figure 7.10 shows both the dark and illuminated J - V characteristics of the crystalline Si and *a*-Si:H solar cells. The difference between a diffusion type device and a drift type device is reflected in the behaviour of the dark and illuminated J - V curves as illustrated in Figure 7.10. In crystalline Si solar cells, the carriers, which are generated outside the depletion region of the solar cell, determine the photocurrent. These are carriers that are generated in the bulk of a wafer, which is electrically neutral. Therefore, the photocurrent is almost independent on the applied voltage. In forward bias, the total current of the solar cell under illumination, which is a sum of the photocurrent and the dark current, is smaller than the dark current. Therefore, the dark and illuminated curves do not cross. In the case of *a*-Si:H solar cells, the photocurrent is determined by the carriers generated in the intrinsic layer of the cell, which is part of the depletion region of the solar cell. The photocurrent, that is mostly the drift current, depends on the electric field in the depletion region and therefore also on the applied voltage. At a certain forward bias voltage, V_T , the photocurrent is zero. For voltages higher than V_T the electric field in the depletion region is reversed, as a result of which the photocurrent is added to the dark current. The resulting total current of the solar cell is higher than the dark current and the dark and illuminated curves cross.

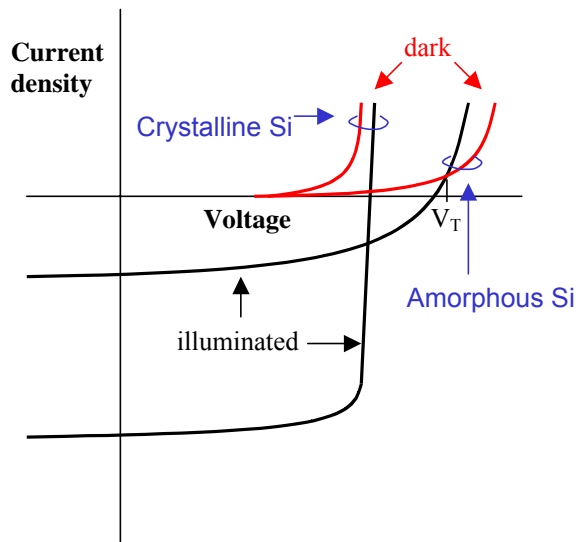


Figure 7.10. The dark and illuminated J - V characteristics of the c-Si and a -Si:H solar cells.

Figure 7. 11 shows the difference in the J - V characteristics of a crystalline Si solar cell and an a -Si:H solar cell measured under standard AM1.5 illumination conditions. Both J - V curves represent the best results in the field of crystalline Si and a -Si:H solar cells at present and are achieved by the University of New South Wales (UNSW) in Australia and United Solar Systems Corporation (USSC) from the United States of America, respectively. The external parameters of the cells are reported in Table 2. It should be noted that the crystalline Si solar cell generates a very high short circuit current in comparison to a -Si:H solar cell and also the fill factor is higher. On the other hand due to a higher band gap the a -Si:H solar cell achieves a higher open circuit voltage.

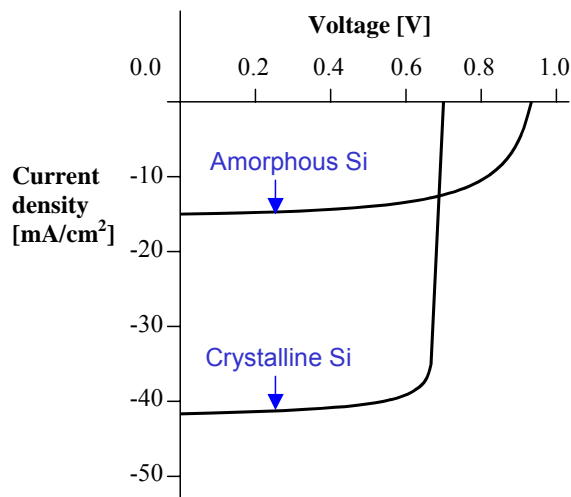


Figure 7. 11. The J - V characteristics of the c-Si and the single junction a -Si:H solar cells. The external parameters of the solar cells are in Table 2.

Table 2. The external parameters of the best laboratory crystalline Si and a-Si:H solar cells.

	J_{sc} [mA/cm ²]	V_{oc} [V]	Fill factor	Efficiency [%]
UNSW mono c-Si PERL structure	42.2	0.706	0.828	24.7
USSC a-Si:H p-i-n structure	14.3	0.965	0.672	9.3

7.6.2 Single junction a-Si:H solar cell

A typical a-Si:H solar cell is represented by a single junction solar cell. There are two configurations of the single junction a-Si:H solar cell, namely the *p-i-n superstrate* configuration and the *n-i-p substrate* configuration. The type of configuration reflects the deposition sequence of the a-Si:H based layers. In the *p-i-n* configuration the *p*-type layer is deposited first, then the intrinsic layer and the *n*-type layer is deposited as the last one. In the *n-i-p* configuration the sequence of the deposition is vice versa. When glass or another transparent material is used as a substrate, the *p-i-n* configuration is used. In case of a stainless steel or another non-transparent material, the *n-i-p* deposition sequence is applied. The reason for these two approaches is that the light enters the bulk of a solar cell through the *p*-type layer. This will be explained below.

A single junction *p-i-n* a-Si:H solar cell is deposited on glass substrate coated with a TCO. The TCO forms the top electrode and aluminium or silver is used as the bottom electrode. Since only the a-Si:H intrinsic layer contributes to the current generation, the optimal optical design of the cell structure maximises absorption in the intrinsic layer and minimises absorption in all the other layers. A standard a-Si:H *p-i-n* cell that has been fabricated at Delft University of Technology and at Utrecht University is designed to have a thin (0.01 μm) *p*-type layer; a thicker (0.45 μm) intrinsic layer; and a thin (0.02 μm) *n*-type layer.

There are some important practical design approaches for making high efficient a-Si:H solar cells schematically depicted in Figure 7.8b. These approaches lead to an enhancement of light absorption in the intrinsic layer of a-Si:H and are commonly described by the term **light trapping**.

- (i) The substrate that is used for deposition of a-Si:H layers is practically always textured. In Fig. 8b glass with textured SnO₂:F as the TCO represents the substrate. The texture introduces rough interfaces into a solar cell. When light enters the solar cell and reaches a rough interface, a part of it will be scattered in various directions instead of propagating in the specular direction. In this way the average light path in a layer is increased and the light absorption is enhanced.
- (ii) In most practical a-Si:H solar cells the light enters the solar cell through the *p*-type layer. The reason for this has to do with the lower mobility of holes in comparison to electrons in a-Si:H. Since most of the photo-generated carriers are generated in the front part of the solar cell, holes have to travel on average shorter distance than the electrons to the respective electrodes. Remember that the photo-generated holes travel towards the *p*-type layer. In this way the collection efficiency of the holes is enhanced.

- (iii) Because the light enters the solar cell through the *p*-type layer there is a substantial absorption in this layer. The photo-generated carriers in the *p*-type layer do not contribute to the photocurrent because the electrons, which are the minority carriers in the *p*-type layer, quickly recombine in this layer. It is therefore desired to minimize the absorption in the *p*-type layer which is realized by alloying the *a*-Si:H with carbon. The *p*-type *a*-SiC:H layer has high optical band gap and is referred to as a **window layer**.
- (iv) In order to accommodate a band offset between the *p*-type *a*-SiC:H and the intrinsic *a*-Si:H layer and to prevent a back diffusion of the photo-generated electrons into the *p*-type layer, thin layers are introduced at the *p-i* interface. These layers are called the **buffer layers**.
- (v) The cell is completed by the back electrode that often consists of a ZnO layer followed by a back metal, usually Ag, on top of the *n*-type *a*-Si:H layer. It has been demonstrated that this combination results in a highly reflective back contact that enhances the absorption of light in the long wavelength region (wavelengths above 600 nm).

7.6.3 Degradation of *a*-Si:H solar cells

Inherent to *a*-Si:H is that it exhibits changes in material properties when subjected to some external excitation such as illumination. The changes can be subsequently removed by annealing the material for a few minutes at 150°C to 200°C. Staebler and Wronski reported in 1977 the first measurements in which they found a decrease in the photoconductivity during illumination and a decrease in the dark conductivity after illumination²⁰. This effect is since then called the **Staebler-Wronski effect**. When solar cells are exposed to illumination a slow degradation of their performance is observed that is related to the Staebler-Wronski effect. The Staebler-Wronski effect is an example of the metastable creation of additional defects in the material under illumination. In solar cells these additionally created defects will act as extra trapping and recombination centres. As a result of the trapping a space charge distribution in the intrinsic *a*-Si:H layer is changed in such a way that the internal electric field is distorted. This leads to lower drift and thus to a lower collection efficiency. Much effort has been spent to find a solution for avoiding the Staebler-Wronski effect in solar cells. There is a continuous search for *a*-Si:H material with stable properties. New deposition techniques are investigated, such as HW CVD, that are expected to deliver more stable *a*-Si:H material.

The performance of *a*-Si:H solar cells decreases during the initial stage of operation due to light-induced degradation. After the initial degradation the performance of the solar cells stabilises. The stabilised performance of high quality solar cells is 70 - 90% of their initial performance. The degradation can be recovered by annealing. Therefore attention has to be paid, whether the reported efficiency of *a*-Si:H solar cells is the **initial efficiency** (as made) or the **stabilised efficiency** (after a degradation test). In different countries different conditions are defined for carrying out the degradation test. In Japan, "temporarily defined stabilised efficiency" is the value after 310-hour-exposure under following conditions: light intensity 1.25 sun, temperature 48°C, and open circuit condition. In the USA the stabilised efficiency is defined as the efficiency after 600 hours of continuous exposure to 1 sun at 50°C at open circuit conditions.

²⁰ D. L. Staebler and C. R. Wronski, *Appl. Phys. Lett.* **31**, 292 (1977).

The best reported initial efficiency for a laboratory single junction a -Si:H solar cell is 13.2% and it was achieved by a Japanese company Mitsui Toatsu. The highest stabilised efficiency is reported by USSC to be 9.3%. An example of illuminated J - V characteristics for the initial and the degraded states of a standard a -Si:H solar cell fabricated at TUD is shown in Figure 7.12. The external parameters of the cell are also reported in Figure 7.12.

7.6.4 Multi-junction a -Si:H solar cells

The degradation problem of a -Si:H solar cells can be partly solved by using thinner intrinsic layers in which case the internal electric field is higher and therefore less sensitive to any distortion. However, using a thinner layer results in a decreased absorption in the solar cell. A solution to obtain cells with a better stability and at least similar absorption as in the case of the conventional single junction solar cells is to stack two or more single junction solar cells with thin intrinsic layers on top of each other. This approach is called a **multi-junction** concept. In case of two junctions stacked on top of each other we talk about a **tandem** or **double-junction** solar cell, a stack of three junctions is named a **triple-junction** solar cell. The total thickness of the multi-junction solar cell is similar to a conventional single junction solar cell, but each component cell is thinner and therefore less sensitive to light-induced defects. An additional advantage of a multi-junction cell structure is that each component cell can be tailored to a specific part of the solar spectrum, thereby extending a usable part of the spectrum and increasing the solar cell conversion efficiency. At present the tailoring is realised by implementing a -SiGe:H. This effect is illustrated in Figure 7.13. Intrinsic a -Si:H has an optical band gap of ~ 1.70 eV and absorbs only photons with energies above 1.70 eV efficiently. The photons with the lower energies are not absorbed and thus lost for the energy conversion. A part of the photons with energies lower than 1.70 eV can be absorbed by a -SiGe:H layer that has an optical band gap of 1.45 eV. Tuning of the response to the solar spectrum is achieved by varying the concentration of germanium in a -SiGe:H, thereby lowering the optical band gap of the material. We call the implementation of materials with different optical band gaps for the active layers in multi-junction solar cells a **multi-band gap** approach. Most of current high efficient solar cells are based on the multi-junction and multi-band gap approach.

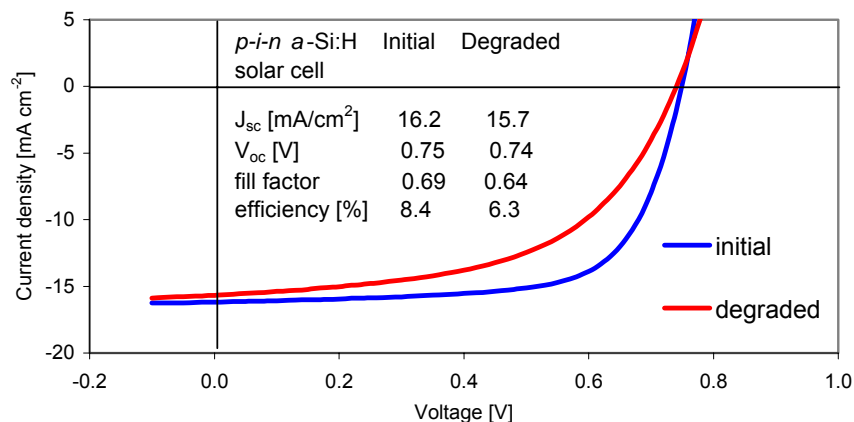


Figure 7.12. The initial and degraded illuminated J - V characteristic of a single junction p - i - n a -Si:H cell fabricated at Delft University of Technology.

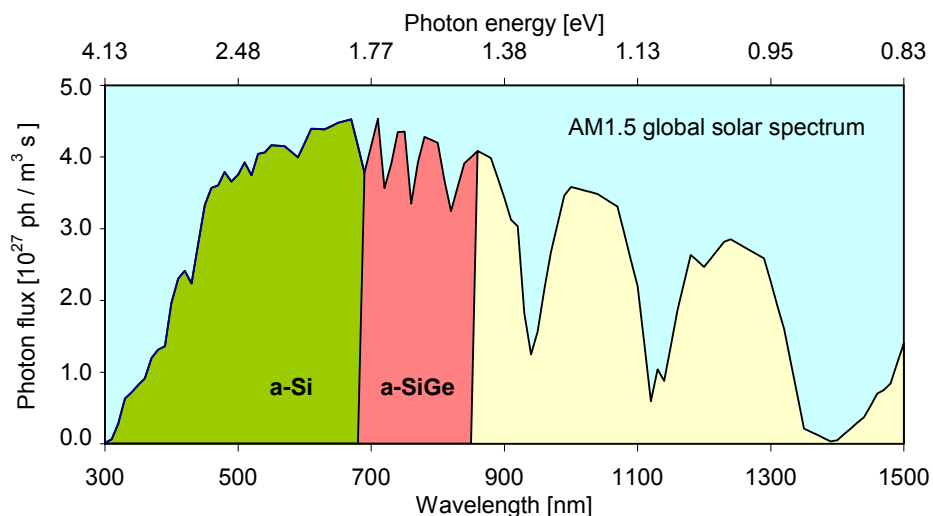


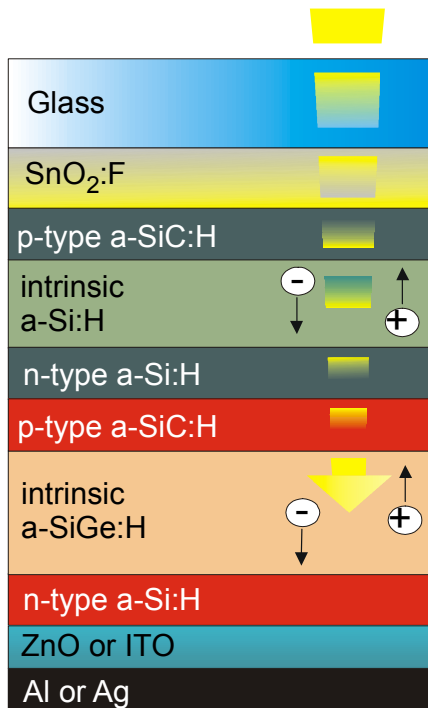
Figure 7.13. The AM1.5 global solar spectrum and the photons of the spectrum that are utilised by a -Si:H and by a -SiGe:H.

The multi-junction solar cell structure is far more complex than a conventional single junction solar cell. There are two crucial requirements for successful operation of the multi-junction solar cell: (i) the current generated at the maximum power point has to be equal in each component cell and (ii) a **tunnel-recombination junction** (TRJ) between the component cells has to feature low electrical and optical losses.

The first requirement reflects the fact that the component cells function as current sources that are connected in series. Therefore it is needed that each component cell generates the same current. The generated current depends mainly on the thickness of the intrinsic layer. In order to generate the same current, the thickness of the intrinsic layer of each component cell needs to be carefully adjusted, thereby taking the profile of photogenerated carriers, so called generation profile, in the cell into account. The second requirement concerns the interface between the component cells. This interface is in fact an n - p diode, which is connected in reverse, when the component cells operate in forward conditions. An ohmic contact between the component cells instead of a rectifying contact is required for proper operation of the solar cell. The problem can be resolved by fabricating a so-called tunnel-recombination junction. This junction ensures that the electrons that arrive at the n -type layer of the top cell and the holes that arrive at the p -type layer of the bottom cell fully recombine at this junction. The recombination of the photo-generated carriers at this interface keeps the current flowing through the solar cell. A very high electric field in this reverse biased p - n junction facilitates tunnelling of the carriers towards the defect states in the centre of the junction. The effective recombination of the carriers takes place through these states. A tunnel-recombination junction is usually realised by using microcrystalline silicon for at least one of the doped layers and/or to increase the defect density by incorporating a thin oxide layer at the interface between the two component cells.

An example of an a -Si:H/ a -SiGe:H tandem cell is shown in Figure 7.14. The illuminated J - V characteristic and the external parameters of a a -Si:H/ a -SiGe:H tandem cell

fabricated at Delft University of Technology are presented in Figure 7.15. The *a*-Si:H component cell absorbs photons with energies above 1.70 eV, photons with lower energies, which pass through the *a*-Si:H top cell, get a chance to be absorbed in the bottom cell by *a*-SiGe:H.



Tandem a-Si:H/a-SiGe:H cell

J_{sc} [mA/cm ²]	8.74
V_{oc} [V]	1.49
fill factor	0.67
efficiency [%]	8.7

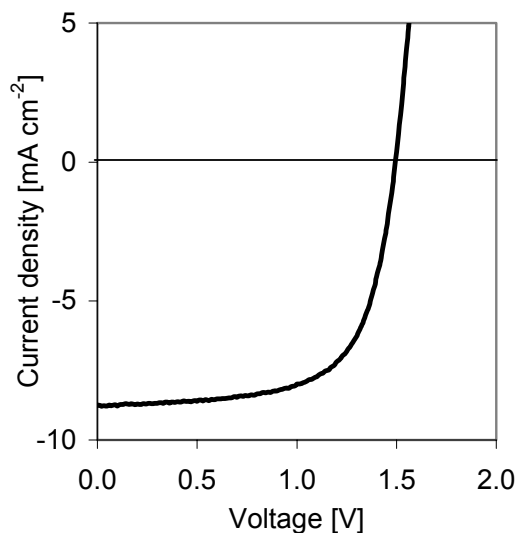


Figure 7.14. Typical structure of an *a*-Si:H/*a*-SiGe:H tandem cell.

Figure 7.15. The illuminated *J-V* characteristic of a tandem *a*-Si:H/*a*-SiGe:H cell fabricated at Delft University of Technology.

In order to achieve current matching, the thickness of the intrinsic *a*-Si:H layer in the top cell is ~100 nm and the thickness of the intrinsic *a*-SiGe:H layer in the bottom component cell is ~150 nm. It means that the total thickness of a tandem cell is less than that of a single junction *a*-Si:H solar cell, in which the thickness of the intrinsic layer varies between 300 to 450 nm. As explained above, the use of *a*-SiGe:H for the intrinsic layer of the bottom cell in a tandem structure enhances the response of the cell in the long wavelength region. On the other hand, the use of *a*-SiGe:H introduces large band offsets near the *p-i* and *i-n* interfaces. For example, the band offset of 0.5 eV exists between a *p*-type *a*-SiC:H layer with a typical optical band gap of 1.95 eV and an *a*-SiGe:H layer with an optical band gap of 1.45 eV. These band offsets are believed to obstruct an effective collection of photo-generated carriers. In order to overcome this, profiling of the germanium concentration is carried out in a region near the interfaces. The term **graded layer** is used to denote the profiled region.

The highest stabilised efficiency for *a*-Si:H based solar cells to date has been demonstrated by USSC with a triple junction structure. This solar cell structure is shown in

Figure 7.16. In order to illustrate the complexity of the solar cell structure, which accommodates the graded layers and different materials for the active layers, a corresponding band diagram of the cell has also been included in Figure 7.16. USSC reported the stabilised efficiency of a small area cell (0.25 cm^2) to be 13.0 %. The initial efficiency of this cell was 14.6 %. Recently, an initial efficiency of 15.2 % was reported by this group, which indicates that further improvement in stabilised efficiency is feasible.

Comparing the external parameters of the single junction (see Figure 7.12) and tandem (see Figure 7.15) solar cells we notice that the J_{sc} is lower while the V_{oc} is higher in case of a tandem cell. This observation is even more pronounced for triple-junction cells. For practical applications, the external parameters of multi-junction solar cells are advantageous in comparison to single junction cells, because the lower current means less loss in the electrodes, especially in the TCO, and the higher output voltage allows more flexible design of a module with required voltage.

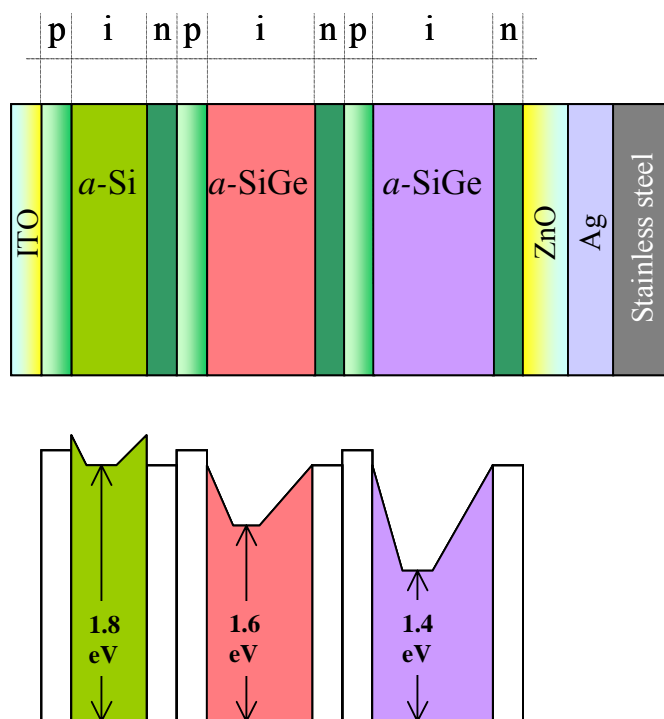


Figure 7.16. A triple-junction solar cell with a corresponding schematic band diagram.

7.7 Fabrication of thin-film silicon PV modules

7.7.1 Thin-film silicon PV modules

Power that is delivered from a small area laboratory cell is not enough in practical applications. Therefore, solar cells are connected with each other in series and/or parallel to form a module that delivers a required power or voltage. The solar cell performance that is first optimised on a laboratory scale with a cell area ranging from 1 to 100 cm² is difficult to obtain on a module, which has an area 1.000 cm² and more. Several requirements need to be fulfilled on a module level. The uniformity and homogeneity over the deposited area must be good. The area loss due to encapsulation, patterning, and current carrying grid lines and the electrical loss due to TCO and grid lines resistance should be minimal. Concerning conversion efficiency, one has to be careful to distinguish among the reported values, because there is misleading discrepancy between:

- laboratory record mini-cells (size below 1 cm², no patterning)
- R&D modules, not encapsulated and not produced in large quantities (size of 1 square-foot)
- standard commercial modules

Furthermore, attention has to be paid whether the efficiency value is the *initial* efficiency of the cell (as made) or the *stabilised* efficiency (after a degradation test).

A key step to practical industrial production of *a*-Si:H solar cells was the development of the monolithically integrated type of *a*-Si:H solar cell⁶, in which several subcells, deposited on one substrate, are connected in series, as shown in Figure 7.17. The integration of the subcells can be obtained by using conventional masking techniques or laser scribing. Using the monolithic integration of *a*-Si:H solar cells, a desired output voltage from a single substrate can be easily achieved. The process steps for the integration of the subcells can be easily implemented in the whole fabrication process of a module. This gives *a*-Si:H technology a great advantage in comparison with single crystal silicon module technology, where the subcells are mechanically connected with each other.

The first commercial *a*-Si:H solar cells were put on the market in 1980 by the Japanese companies Sanyo and Fuji Electric. Their size was typically a few square centimetres and these cells were applied in consumer electronics such as calculators. Since then the manufacturing technology of *a*-Si:H solar modules has experienced a rapid advance in increasing the module size and the efficiency. In 1999 the total production of *a*-Si:H modules was 25 MWp that represented 12.3% of the world total PV module production. There are several facilities in the world that manufacture large area *a*-Si:H modules. In 2001 several mass-production lines were in operation such as by Kaneka in Japan (20 MWp/year), BP Solarex (10 MWp/year) and USSC (5 MWp/year) in the USA. Several companies work on the basis of a pilot line such as Phototronics in Europe, Fuji Electric and Sanyo in Japan.

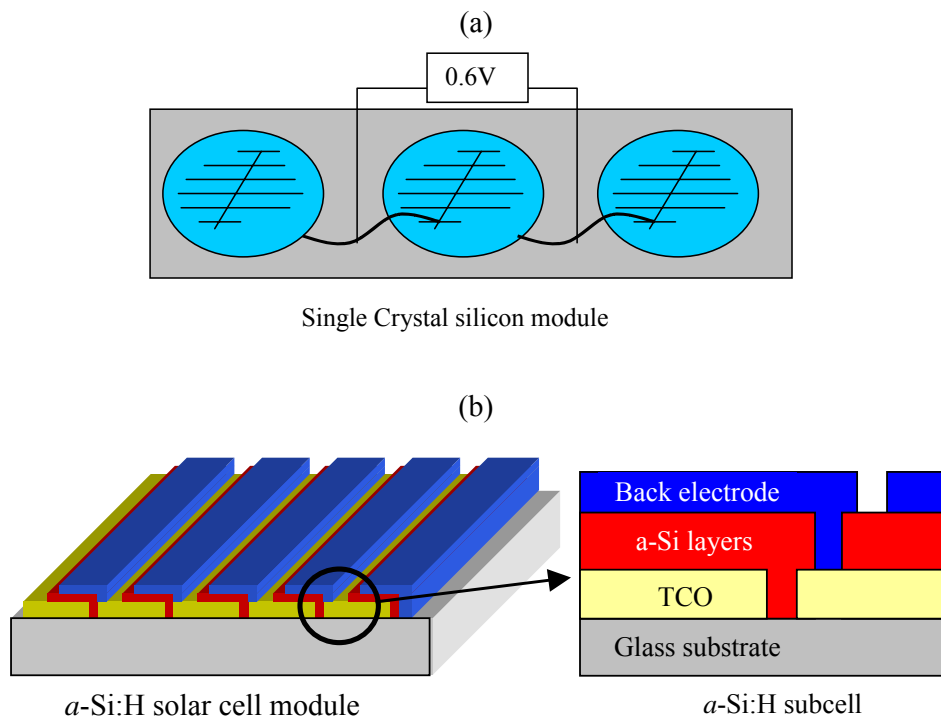


Figure 7.17. Schematic representation of a series interconnection. (a) Mechanically interconnected single crystal silicon cells and (b) Monolithically integrated *a*-Si:H subcells.

At present, glass-plates or stainless steel sheets are used as the substrates in production. The choice of the substrate material influences the production technology, though the principal steps of the production process remain the same for both. In case of glass substrates the *p-i-n* deposition sequence is used, in case of stainless steel the *n-i-p* sequence process takes place. The different sequence has influence on some of the technological steps. The main steps in fabricating the solar cells are:

- substrate preparation
- TCO front electrode deposition
- deposition of *a*-Si:H layers
- back electrode deposition
- final assembly (encapsulation, framing, and testing)

One of the important requirements for a company to stay competitive in the solar cell business is to be technologically independent. This is a driving force for the companies to have all necessary technologies available. Central to each of the production lines is the PECVD reactor, whose design determines throughput, flexibility to cell design variations, quality and uniformity of the layers and defect density levels. Most producers who use TCO coated glass substrates strive to have their own TCO deposition in order to be independent of the suppliers. Having an own TCO deposition machine enables them to control the quality of the TCO that is crucial for overall performance of solar cells. The commercial *a*-Si:H modules consist of monolithically integrated cells. The series interconnection on the substrate is achieved during the construction of the cell structure by including two or more laser scribing steps between depositions of the respective layers. The laser cutting selectively removes

narrow lines (width 50 to 150 μm) of material in order to limit the area losses. The laser scribing is also a speed limiting step in the production line. Usually, pulsed Nd:YAG lasers are used for scribing the films. The final product must be well protected against the atmospheric influence to prolong its lifetime. Several encapsulation methods are used for the purpose of protection. Most common method is to use a polymeric film ethylene/vinyl acetate (EVA) as the cover of the module on top of which a glass sheet is placed. An increasing attention is paid to framing of the modules as *a*-Si:H solar modules are becoming an attractive element for building applications.

7.7.2 PECVD deposition systems

Since the *a*-Si:H and/or μc -Si:H layers form the heart of the solar cell, the way these layers are produced at industrial level is described in more detail. The standard industrial deposition technique of *a*-Si:H and μc -Si:H is the PECVD method. There are several configurations of the PECVD reactors that are used for production.

(A) *Single chamber system*

The deposition of all *a*-Si:H layers is carried out in a single reaction-chamber. This system has the advantage that there is no transport of substrates under vacuum conditions. If a load lock chamber is used, a simple form of linear transport is sufficient. The substrates can have a very large size, and can be handled as mounted in a plasma box. The capital investment is low compared to the other configurations. A disadvantage is that production may take a long time since several purge and pump-down steps are needed to obtain well defined consecutive depositions of differently doped and undoped layers. There are limited possibilities to apply buffer layers or graded layers at the interfaces. The geometry of the electrodes and the deposition temperature usually cannot be varied for the various layers. This leads to a trade off between the optimum deposition parameters for the individual layers. Therefore, in a single chamber system the solar cell structure will be less than optimal.

(B) *Multi-chamber system*

This system has the advantage of complete control of the level of dopants and other impurities. In this type of system it is possible to produce controlled compositional profiles, with increasing or decreasing concentrations of constituents, without affecting the impurity level of subsequent layers. The deposition temperatures, the internal geometry, and even the discharge frequency can be optimised for each layer individually. The transfer of the manufacturing process from the laboratory to production requires only small adaptations. A disadvantage is that the size of the panels may be limited. Nevertheless, the panels with a size of 40 cm \times 120 cm and 60 cm \times 100 cm have been produced with multi-chamber configuration. Another disadvantage is that the investment is quite large.

Two types of multi-chamber systems are in operation:

(B1) *in-line configuration*

This configuration offers the feasibility to deposit on moving substrates. This leads to extremely good uniformity of the layers over very large areas, an important feature for tandem solar cell structures. As the deposition plasma does not need to be extinguished, an important source of dust and microparticles is eliminated. The throughput of these machines can be very high. However, the equipment cost is very high, because special isolation chambers and vacuum valves are needed to separate the deposition chambers. Furthermore, in-line machines usually take up quite some space. The layer sequence is determined by the

physical configuration of the system and cannot be adapted easily. This reduces flexibility in a multi-layer structure.

(B2) cluster configuration

This configuration is known from the laboratory, but may be the best choice also for (pilot) production. A cluster system has all the advantages of a multi-chamber system. The transition from laboratory experience to production is as small as possible. Modifications in the layer sequence or changes in the number of the layers of the solar cell structure (e.g. from a single junction to a tandem or triple junction) can be made as desired. Apart from this the capital cost is low, because transport and isolation chambers can be shared by many deposition chambers. If a sufficient number of chambers are connected to the transport chamber, production can be continuous even if one of the deposition reactors is down for maintenance. This is in contrast to *in-line* systems, which must be shut down completely if one of the chambers needs maintenance. The area requirement of a cluster system is very modest. The flow of reactive gases is only needed when there is a substrate in the deposition chamber, thus cutting down the base materials usage. Profiled and graded layers are much more easily made than in the case of *in-line* systems.

All of the above production facilities can be used in a *single panel* mode or in a *batch* mode. In the latter mode a number of substrates is loaded at the same time, a principle often applied in a single chamber system to bring the throughput to the required level. Due to the long processing time single chamber systems can only be cost-effective when they are batch-type systems. In multi-chamber systems one usually uses a single panel mode. The panels can be transported in a holder or without support. The latter possibility reduces cross contamination, which may result from the holder. As the number of vacuum chambers is larger and as purging steps can be omitted, the throughput can be approximately equal to that of a single chamber system. Multi-chamber processes can also use batch type mode. Several substrates have to be then transported simultaneously in vacuum. This can be done even without a holder, which however may lead to very complicated transport mechanisms.

(C) Roll-to-roll system

The roll-to-roll process is neither the single chamber nor the multi-chamber method. At present, this process is used by USSC and its affiliates for depositing tandem and triple-junction solar cells. An example of the flexible and framed modules produced by USSC is shown in Figure 7.18. It is potentially a cheap method, but there are some disadvantages. For instance, if the substrate is made of stainless steel, then the series interconnections cannot be done monolithically. A solution is to use the stainless steel merely as a carrier for an insulating plastic substrate. The central part of the line, the machine for the a-Si alloy deposition, consists of a stainless steel web roll-off chamber, six (nine) PECVD chambers for six (nine) layers of the double (triple) junction cell and a roll-up chamber. Stainless steel web, coated with Ag/ZnO, moves continuously through the chambers where the various layers are sequentially deposited. There is an increased risk that cross contamination occurs, since all deposition zones by definition are connected to each other. Since no purging steps can be used as in the single chamber systems, so-called gas gates are used to isolate the adjacent chambers and minimise the adverse effects.



Figure 7.18. Example of USSC flexible and framed a -Si:H solar cell products.

In 1997 a project was started in the Netherlands with the purpose to develop a roll-to-roll production method for a -Si:H thin film solar cells, called the Helianthos project. The production method is based on a novel *temporary-superstrate* concept. This means that a p - i - n a -Si:H structure is deposited on a temporary carrier, which is coated with SnO_2 :F TCO. The aluminium foil serves as a temporary carrier of the solar cell. After deposition of the complete solar cell, including the back contact, the cell is laminated on a permanent carrier. By removing the aluminium foil, light can enter the cell through the top TCO layer. A wide variety of transparent encapsulants can be used to finalize the product that can be flexible or rigid. The Helianthos project is carried out by Utrecht University, Delft and Eindhoven Universities of Technology, the Netherlands Organization of Applied Scientific research, and the multinational corporation Akzo Nobel. The feasibility of the new temporary-superstrate concept has been demonstrated by depositing a solar cell with 6% initial efficiency. A roll-to-roll pilot plant is expected to be in operation in 2002.

For those readers who are interested to learn all aspects of a -Si:H and μc -Si:H solar cell technology in detail a book on “Amorphous and Microcrystalline Silicon Solar Cells” written recently by Schropp and Zeman¹⁷ is recommended.